Distribution Category:
Magnetic Fusion Energy
(UC-420)

ANL/FPP/TM--242

DE89 016704

ANL/FPP/TM-242

ARGONNE NATIONAL LABORATORY
9700 South Cass Avenue
Argonne, Illinois 60439-4801

EROSION/REDEPOSITION ANALYSIS OF THE ITER DIVERTOR

by

J.N. Brooks

July 1989

Work supported by

Office of Fusion Energy
U.S. Department of Energy
Under Contract W-31-109-Eng-38

TABLE OF CONTENTS

LIST OF FIGURES

LIST OF TABLES

EROSION/REDEPOSITION ANALYSIS OF THE ITER DIVERTOR

by

Jeffrey N. Brooks

ABSTRACT

Sputtering erosion of the proposed ITER divertor has been analyzed using the REDEP computer code. A carbon coated plate at medium and low plasma edge temperatures, as well as beryllium and tungsten plates, have been examined. Peak net erosion rates for C and Be are very high (~20-80 cm/burn-yr) though an order of magnitude less than the gross rates. Tritium buildup rates in co-deposited carbon surface layers may also be high (~50-250 kg/burn-yr). Plasma contamination, however, from divertor sputtering is low ($\lesssim$.5%). Operation with low Z divertor plates, at high duty factors, therefore appears unacceptable due to erosion, but may work for low duty factor (~2%) "physics phase" operation. Sweeping of the poloidal field lines at the divertor can reduce erosion, by typical factors of ~2-8. A tungsten coated plate works well, from the erosion standpoint, for plasma plate temperatures of ~40 eV or less.

1. INTRODUCTION

The lifetime of a tokamak reactor impurity control surface remains one of the critical issues for fusion. In particular, a divertor plate is subject to severe erosion by sputtering and disruptions. As part of the International Tokamak Engineering Reactor (ITER) study[1], the sputtering erosion of a double null divertor plate, operating in the high recycling regime, has been analyzed. The purpose of this work is twofold: (1) to compute engineering design data for ITER, and (2) to generally advance the science of sputtering erosion calculations.

The analysis uses the REDEP erosion/redeposition code.[2] This code has been updated with numerous plasma scrapeoff, boundary, sputtering models, and numerical methods, since its original development. The code has been partially verified by comparing code predictions to measured erosion rates and plasma contamination levels, for the TEXTOR ALT-1 limiter,[3] and the TFTR bumper limiter.[4,5] The comparisons have been good, but additional verification is needed, particularly on a shot-to-shot basis. This work is being planned. On the basis of the comparisons with experiment, the code results for ITER should probably be regarded as reliable concerning broad trends. Detailed reliance, however, on specific numbers should be done with caution.

The ITER design calls for steady state current drive. This may force the plasma temperature at the divertor plate to be too high ($\gtrsim$50 eV) for high Z plate materials. For this reason the focus of the analysis is on carbon which can operate without self-sputtering runaway for all plasma edge temperatures. Detailed calculations of physical sputtering for off-normal incidence, hydrogen saturated carbon, have been used in the analysis. Chemical sputtering has been analyzed using a simplified model. Beryllium has been examined as an alternative to carbon, at all plasma conditions, while tungsten has been examined as a low temperature alternative.

2. PLASMA MODEL

The divertor geometry is modeled as shown in Fig. 1. The lower outboard divertor plate is analyzed. Top and bottom outboard plates of a double-null divertor should have identical erosion properties while inboard plate erosion should be less severe due to a lower particle flux. (It is estimated that 40% of the edge particle current goes to each outboard plate and 20% to each

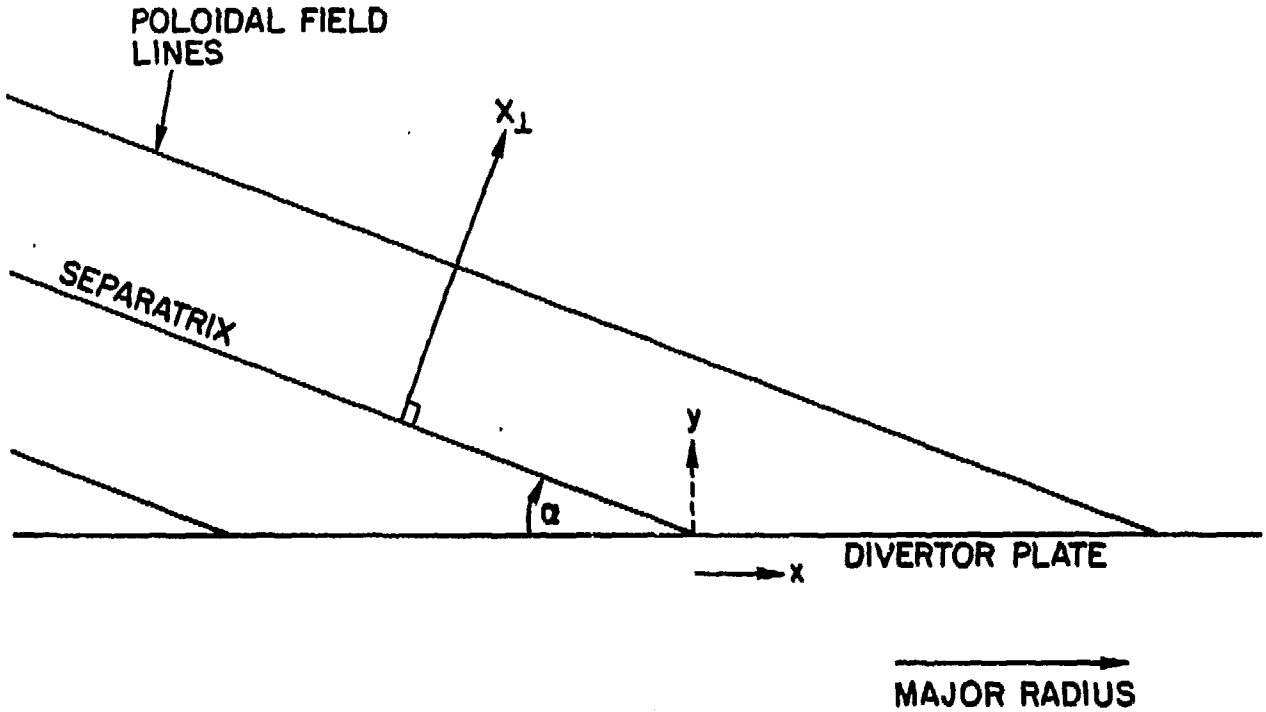

Figure 1. Divertor geometry model.

inboard plate.) The plate is tilted at an angle "α" to the poloidal field lines, which are assumed to be parallel in the vicinity of the plate ($y \leq 3$ cm). The coordinate "$x_\perp$" is the perpendicular distance from the separatrix field line.

The plasma model for the REDEP calculations is shown in Table 1. This model is based on results of a series of 2-D plasma transport code calculations by Braams[6] for the high recycling divertor regime, and represents an approximation to the transport code results for the plasma near the divertor plate. Calculations by Harrison[7] show similar results. The key features of the plasma model are as follows: exponential particle and energy profiles, ion temperature lower than electron temperature, short temperature e-folding distance, and broad density profile. The sensitivity of the erosion results to the e-folding distances and other parameters has been assessed.

DEGAS code calculations[8] indicate that the charge exchange (CX) flux to the divertor is about 25% of the D-T ion flux. The CX energy spectrum, however, is too low to significantly affect physical sputtering, and so CX is not included in the REDEP calculations. Chemical sputtering of carbon, however, could be enhanced by the CX flux.

A further part of the plasma model is that a sputtered particle reaching 3 cm above the plate ($y = 3$ cm) before being ionized is assumed to be lost to the plasma (via the stagnant or flow-reversed fluid flow characteristic of a high recycling regime). Such particles are assumed to be thermalized and returned to the divertor plate in proportion to the D-T flux. There is, in fact, very few sputtered particles reaching even $y = .5$ cm. The erosion results were found to be fairly insensitive to this parameter.

3. REDEP CODE

The REDEP code computes the sputtering, transport, ionization, and redeposition of sputtered impurities for a limiter or divertor. The basic code methodology is described in Ref. (2). For the ITER analysis, a 2-D version of the code is used since the divertor is toroidally symmetric. The following brief discussion can serve to illustrate several elements of the present analysis. Figure 2 shows the geometry pertaining to sputtered particle transport. The divertor plate, at one toroidal location, lies along the x axis. The z axis, at $x = 0$, lies along the toroidal direction. The

Table 1. Plasma Edge Model for MEMEP Calculations

Electron density*	$N_e = N_{e_o} e^{-\lvert x_1 \rvert / \delta_N'}$
Electron temperature*	$T_e = T_{e_o} e^{-\lvert x_1 \rvert / \delta_T'}$
Ion temperature*	$T_i = 0.15\ T_e$
Heat flux, on tilted divertor plate	$q = q_o e^{-\lvert x_1 \rvert / \delta_E'}$
D-T particle flux, on tilted divertor plate	$\Gamma_{DT} = \Gamma_{DT_o} e^{-\lvert x_1 \rvert / \delta_p'}$
Helium flux	$\Gamma_\alpha = f_\alpha\ \Gamma_{DT}$
Sheath potential	$e\phi = 3\ KT_e$
where:	$\Gamma_{DT_o} = \dfrac{q_o}{(1 + f_\alpha) 2\ KT_{i_o} + (1 + 2 f_\alpha)\ 6\ KT_{e_o}}$
	$f_\alpha = .05$
	$N_{e_o} = 3 \times 10^{19}\ m^{-3} \left(\dfrac{150\ eV}{T_{e_o}}\right)^{1.5}$
	$q_o = \dfrac{10\ MW}{m^2} \left(\dfrac{\sin \alpha}{\sin 20^\circ}\right)$
	$\delta' = \begin{cases} \delta, & x_1 \geq 0 \\ 0.5\ \delta, & x_1 < 0 \end{cases}$
	$\delta_T = 3$ cm, $\delta_p = 6$ cm
	$\delta_N = 100$ m, $\delta_E = 2$ cm

* At divertor plate.

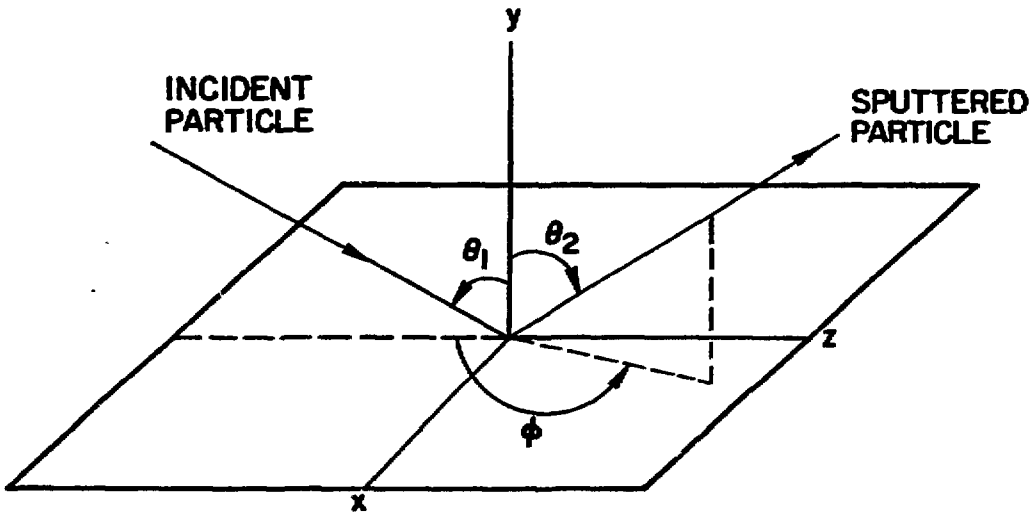

Figure 2. Sputtered particle geometry.

redeposited flux to a divertor point, due to scrapeoff zone ionization of sputtered surface atoms, is found by integrating over all divertor points and sputtered particle angular and energy distributions as follows:

$$\Gamma_{Z_L}(x) = \int_{\phi=0}^{2\pi} \int_{\theta=0}^{\pi/2} \int_{E=0}^{\infty} \int_{x'=x_a}^{x_b} \frac{\Gamma_{Z_s}(x')}{\lambda} f(\phi,\theta,E) \exp\left\{ - \int_0^r \frac{dr'}{\lambda} \right\} d\phi \sin\theta \, d\theta \, dE \, dx' \qquad (1)$$

where $\Gamma_{Z_s}(x')$ is the sputtered flux at point x', f is the probability density function for sputtering at an azimuthal angle ϕ, elevation angle θ, and energy E,

$\lambda = \lambda(x_1) = \frac{V_o}{N_e \langle \sigma v \rangle}$, is the local mean free path where

$$\frac{1}{2} M_z V_o^2 = E,$$

M_z is the impurity mass, $\langle \sigma v \rangle$ is the rate coefficient for electron impact ionization, $r=r(x,x',\theta,\phi)$ is the distance from point x' to the field line intersecting point x, and x_a, x_b are the divertor boundaries.

The redeposited flux is equal to the sum of the scrapeoff ionized flux, Γ_{Z_L}, and the core plasma flux. The sputtered flux, Γ_{Z_s}, results from hydrogen and helium sputtering and self-sputtering due to redeposited material (see Ref. 2). Equation (1) defines a set of integral equations for the sputtered flux at each point. The REDEP code solves the series of integral equations by iteration using the finite difference method. It was found necessary to use a very fine spatial grid for the present analysis where mean free paths are very short in relation to the divertor width. A total of about 10^6 difference-points per computation are used.

4. SPUTTERING DATA

A key feature of divertor sputtering is the off-normal angle of incidence expected for most impinging ions. Based on sheath code results[4,9,10] for a glancing angle magnetic field geometry, the following incidence angles are used to compute sputtering coefficients: $\phi = 0°$ for all particles; $\theta_1 = 60°$ for D, T, He, and Be; $\theta_1 = 50°$, or $60°$ for C (depending on the charge state); and $\theta_1 = 0°$ for tungsten.

For long pulse machines a carbon divertor surface can be expected to be saturated with hydrogen.[11] The hydrogen concentration may play an important role in limiting the self-sputtering coefficient to less than unity, for oblique incidence angles.[4] There is little or no measured data available for these conditions. For these calculations, physical sputtering coefficients for carbon were computed using the model described in Ref. (4), evaluated for hydrogen saturated conditions. (This model yields a peak self-sputtering coefficient of about 0.6, and a D-T sputtering coefficient of .04 at the separatrix, for an edge temperature of 150 eV.)

Sputtering coefficients for Be and W were computed using the DSPUT code.[12] The latter is based on a semi-empirical fit to available data and should provide a reasonable estimate for the present purposes. However, an issue to be resolved for beryllium is whether the self-sputtering coefficient is in fact less than unity for all incidence angles; experimental data is required.

Sputtered particle angular and energy distributions were treated as having the following form:

$$f(\phi,\theta,E) = f_1(\phi)\, f_2(\theta)\, f_3(E) \qquad (2)$$

For carbon, data from the ITMC Monte Carlo Code[13] (a code similar to TRIM) was used to generate data for the functions in Eq. (2). This data was generated for deuterium and carbon impinging on carbon, for the impinging angles described above, and for a representative range of energies. The code results for deuterium are used for tritium and helium. The data shows an approximately cosine distribution in θ i.e.:

$$f_2(\theta) = \frac{1}{2}\cos\theta \ ,$$

and so is similar to the normal incidence case. The ITMC results show substantial specular sputtering, i.e., strongly peaked in the $\phi = 180°$ direction; this data is used in REDEP but is not as significant for the toroidally symmetric divertor problem treated here than it would be for a non-symmetric case (e.g. limiter at one toroidal location). Some of the ITMC computed energy distributions are shown in Fig. 3. As shown, the Thompson model[14] is a good fit to the self-sputtering energy distribution.

Because of their similar mass, and in the absence of other data, the same distribution functions for carbon were used for Be. Since tungsten tends to impinge at normal incidence, an isotropic distribution in azimuth was used. For tungsten, the Thompson model is used for self-sputtering, while light ion sputtering is treated as monoenergetic emission at one half of the binding energy.

A key assumption used for the REDEP calculations is that the redeposited material adequately sticks to the surface. Also, the redeposited material is assumed to have the same sputtering properties as the original surface. These are better assumptions for the metals than for carbon, for reasons discussed in Ref. (2), though there is, in fact, initial data that show acceptable sticking properties of redeposited carbon, e.g. ref. (15).

5. RESULTS

5.1 Carbon Surface - Physical Sputtering Only

For comparison purposes, a test case with parameters $T_{e_o} = 150$ eV, $\alpha = 20°$, and $q_o = 10$ MW/m^2, is employed as a reference case. The erosion results for this case are shown in Fig. 4. This and most other cases are summarized in Table 2. The computational points in Fig. 4 and other figures are 0.25 cm apart. The separatrix is located at point 81. A 50 cm wide divertor plate is modeled. As shown, the gross erosion rate (D,T, He + self-sputtering) is very high, reaching a peak of ~190 cm/burn·yr. The net erosion rate (sputtering minus redeposition) is much lower, by about a factor of 10. A negative net erosion rate implies a surface growth. The growth rate has important implications for the tritium surface inventory and for the surface temperature. The maximum growth rate is 13 cm/burn·yr. As mentioned, all of these values assume adequate sticking of the redeposited carbon. If there is less than adequate sticking the net erosion rate could approach the gross rate.

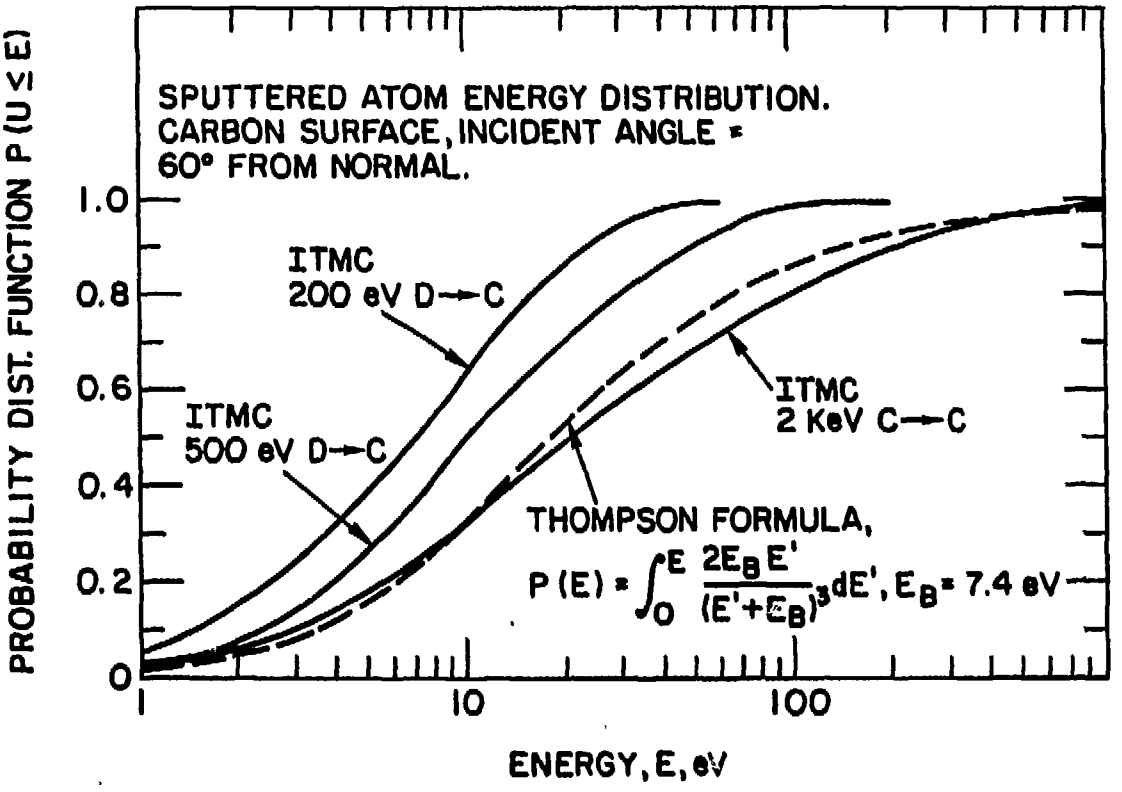

Figure 3. Sputtered carbon energy distribution function, for oblique incidence sputtering. ITMC results from Ref. 13.

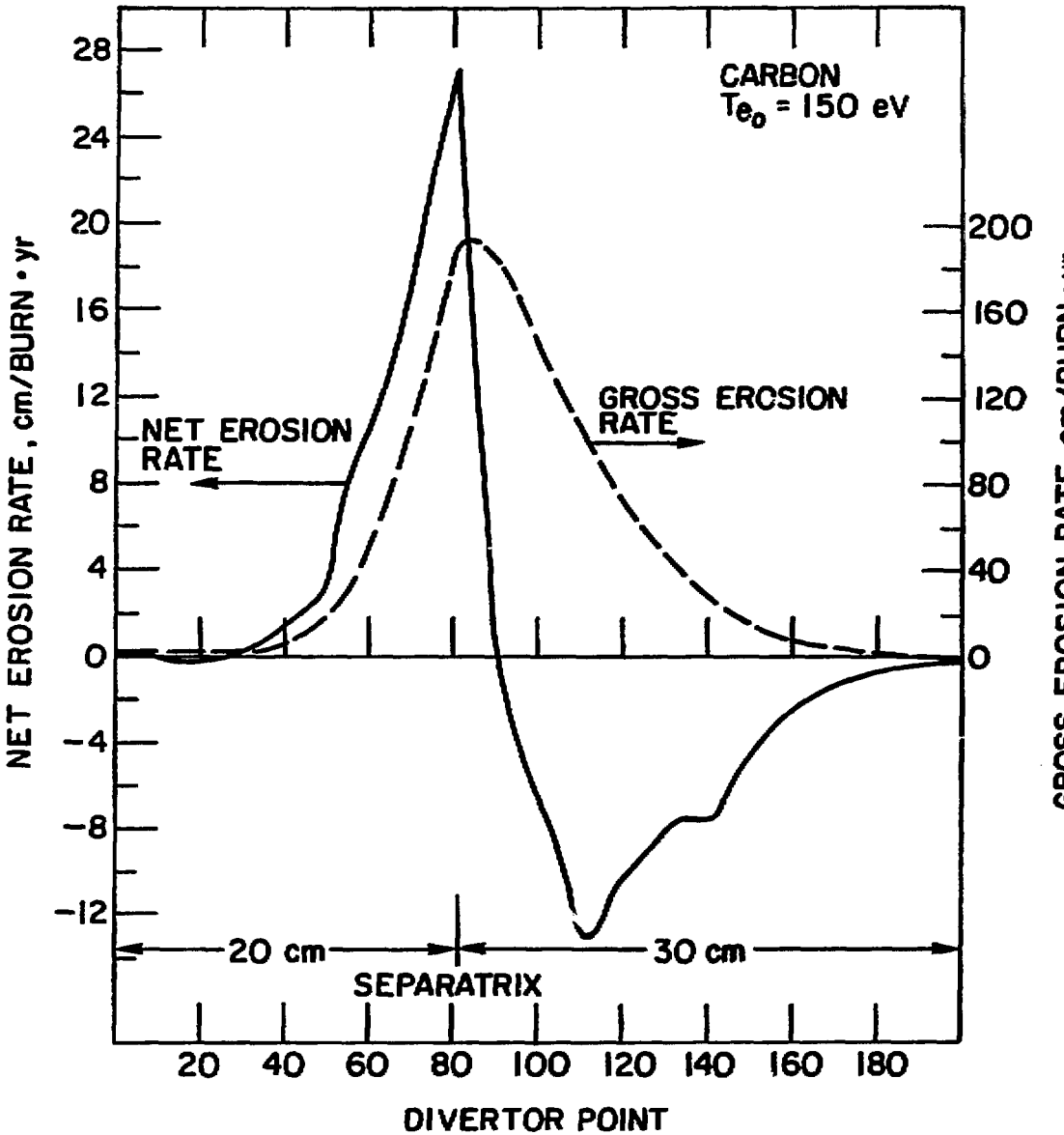

Figure 4. Erosion of a carbon coated divertor plate; for reference case conditions.

Table 2. ITER Divertor Plate REDEP Analysis Summary

Case No.	Divertor Plate Material	Plasma Divertor Temp., T_{e_o}	Other Conditions	Maximum Gross Erosion Rate	Maximum Net Erosion Rate	Minimum Net Erosion Rate	Tritium Co-Deposit. Rate	Comment
1	Carbon	150 eV	(physical sputt. only)*	194 cm/ burn · yr	27 cm/ burn · yr	-13 cm/ burn · yr	155 Kg/ burn · yr	"Reference Case"**
2	Carbon	200		144	23	-12	160	
3	Carbon	100		263	28	-13	135	
4	Carbon	60		329	23	-10	88	
5	Carbon	30		315	17	-10	48	
6	Carbon	150	with chemical sputtering	557	74	-23	260	
7	Carbon	60	with chemical sputtering	1000	52	-24	130	
8	Carbon	150	$\delta_T = \delta_N = 6$ cm	195	20	-6	138	effect of: different profiles
9	Carbon	150	$N_{e_o} = 2 \times N_{e_o}^{REF.}$	209	18	-9	100	higher density
10	Carbon	150	$N_{e_o} = 1/2 \times N_{e_o}^{REF.}$	174	36	-15	213	lower density
11	Carbon	150	$\alpha = 30°$	286	37	-18	140	less tilted plate
12	Carbon	150	$\alpha = 15°$	146	22	-10	165	more tilted plate
13	Carbon	150	$\alpha = 90°$	618	37	-11	35	non-tilted plate
14	Beryllium	150		454	46	-28	40	
15	Beryllium	60		1180	73	-32	33	
16	Beryllium	30		1370	49	-18	18	
17	Tungsten	40		4	.07	-.03	.005	
18	Carbon	150	with sweeping, ± 5 cm	104	15	-9	133	
19	Carbon	150	with sweeping, ± 10 cm	54	8	-7	95	
20	Carbon	150	with sweeping, ± 20 cm	27	4	-4	50	

* All cases physical sputtering only, unless otherwise indicated.

** Reference model: $\delta_T = 3$ cm, $\delta_N = 100$ m, $N_{e_o}^{REF} = 3 \times 10^{19}\ m^{-3} \times (150\ eV/T_{e_o})^{1.5}$, $\alpha = 20°$.

The spatial form of the net erosion rate follows from the exponential dependence of particle flux, and the plate tilt angle. In general, there is a transfer of sputtered plate material from left to right (outboard major radius). The buildup of carbon, on about one half of the plate, may cause a large increase in the reactor tritium inventory if tritium is retained in the co-deposited surface layer. The amount retained can depend on surface temperatures, pulse length, and off-pulse conditioning. A worst-case estimate of the tritium retention was made by assuming a 40% hydrogen to carbon ratio in the co-deposited regions, i.e. 20% T/C. The amount of tritium trapped in one divertor plate was multiplied by a factor of 2.5 to account for trapping on the other outboard plate and the two inner plates. The resulting tritium retention rate is shown in Table 2. For all carbon cases examined, the tritium retention rates are high, indicating a potentially serious problem.

The effect of different plasma edge temperatures on erosion is shown in Fig. 5 and/or Table 2. For these cases the peak heat flux was kept constant at q_o = 10 MW/m^2. There is then a tradeoff between particle flux, which scales inversely with plasma temperature, and sputtering coefficients which decrease at the lower plasma temperatures. In general, the carbon erosion results are qualitatively similar over the 30-200 eV edge temperature range.

5.2 Carbon-Chemical Sputtering

A rigorous analysis of chemical sputtering erosion/redeposition is difficult, at this time, because of a lack of information about critical boundary related phenomena including details of the hydrocarbon breakup and transport, charge states of the redeposited carbon, and the effect of a high local carbon concentration on the sheath and boundary plasma parameters. An approximate analysis, however, as reported here, should give a reasonable insight into the trends expected for chemical sputtering. This analysis has two main assumptions: (1) all chemically sputtered carbon is redeposited at the point of origin, and (2) the carbon so redeposited causes self-sputtering, which can then be treated by the code in the "standard" manner. Assumption (1) is based on the very short mean free paths for chemical sputtered material, e.g. $\lambda \approx 3 \times 10^{-4}$ m for 0.1 eV CD_4, for T_{e_o} = 150 eV. To compute the self-sputtering caused by redeposited, chemically sputtered carbon, a charge state of unity is used. This is a best-case since it minimizes sheath-

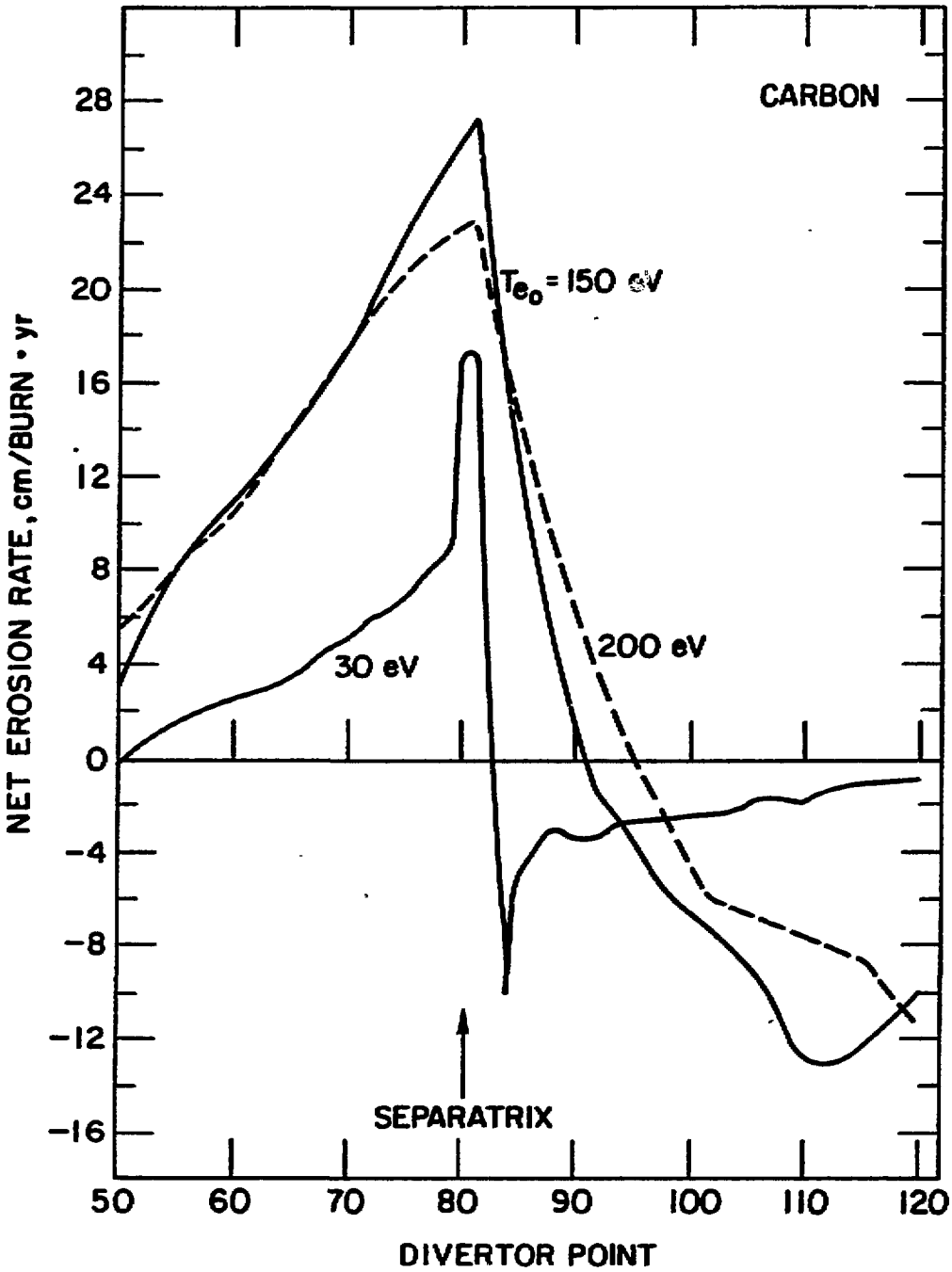

Figure 5. Carbon erosion for different plasma edge temperatures.

acquired energy. (a charge state of 3 is typical of redeposited physically sputtered particles.)

Chemical sputtering was analyzed for a pyrolytic graphite divertor surface. The surface temperature along the plate is computed as a function of the heat flux according to the following:

$$T_s = \begin{cases} 378 + 56\left(\frac{q}{10^6} - 1\right) + .92\left(\frac{q}{10^6} - 1\right)^2, \ ^oC, \ q \geq 10^6 \ \frac{W}{m^2} \\ 378^oC, \ q < 10^6 \ \frac{W}{m^2} \end{cases}$$

where q is the surface heat flux as specified in Table 1. Chemical sputtering coefficients were computed using measured values,[16] where available, and scaling for particle energies where data is unavailable. The resulting sputtering coefficients (average of D → C, T → C, chemical and physical) for T_{e_o} = 150 eV, range from a peak of ~ .2 near the separatrix to ~ .04 at the plate boundaries.

Chemical sputtering erosion results are shown in Fig. 6. The gross erosion exhibits a broader peak than for the physical-sputtering-only case. The net erosion rate, peaking at ~75 cm/burn·yr is about three times higher than the peak for physical-sputtering-only. Charge exchange neutral sputtering (not included) could further increase the erosion rate.

At T_{e_o} = 60 eV with chemical sputtering, the gross erosion rate (see Table 2) increases but the net rate is less than at 150 eV, due to a higher redeposition fraction of the self-sputtered carbon atoms.

5.3 Model Variations

Cases 8-13 of Table 2 were run to assess the effect of model variations. Case 8 has a broader temperature profile and a narrower density profile than the reference case. This results in a somewhat more uniform gross sputtering profile and a reduced peak net erosion rate. Cases 9-10 have different electron densities. As expected, a higher density results in more local redeposition due to shorter mean-free-paths, and hence less net erosion. A lower density has a converse effect.

Cases 9-10 are also equivalent to a change in the ionization rate coefficients by the same factors, e.g. case 9 is equivalent to a case with the reference-case density but with the rate coefficients higher by a factor of

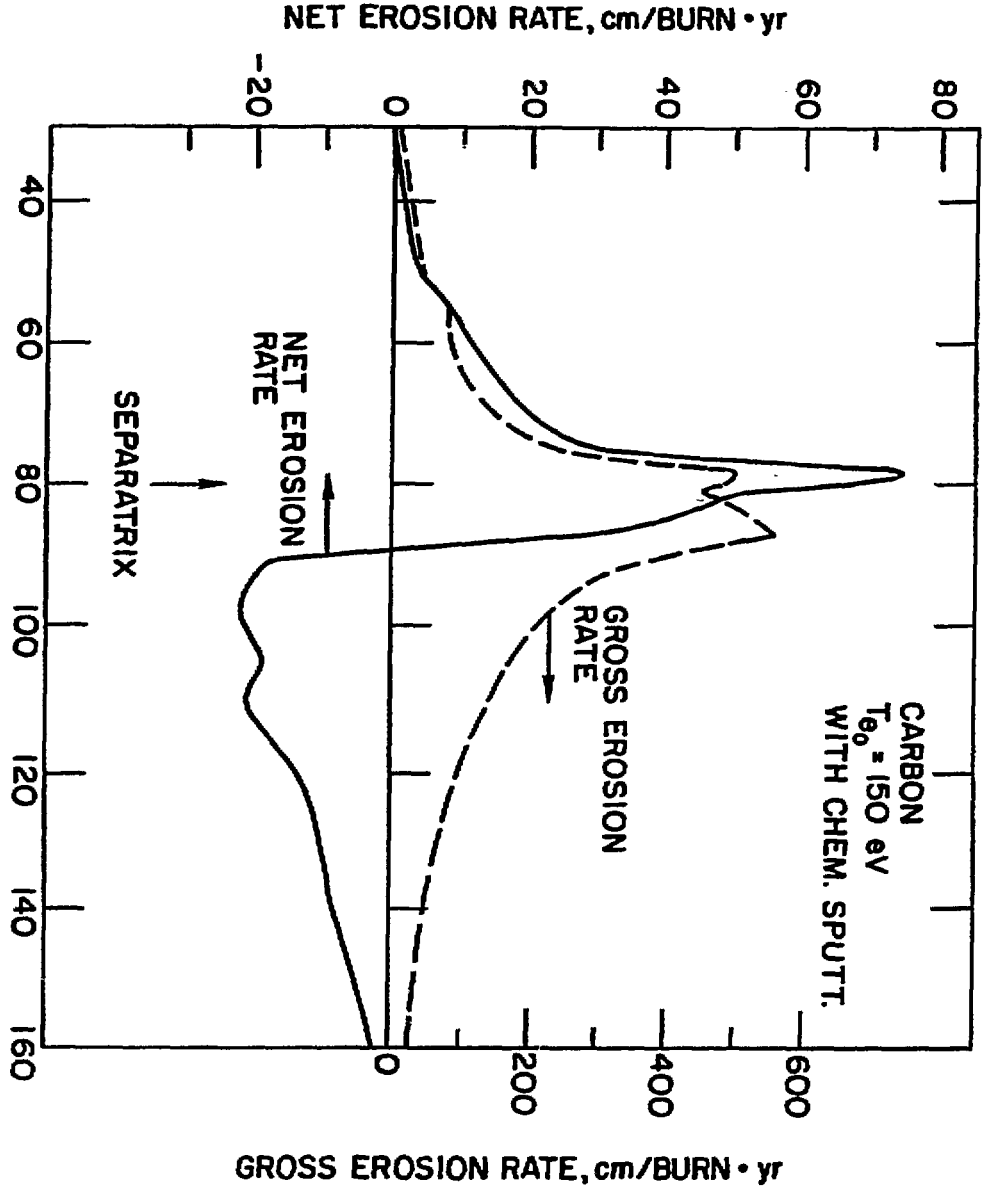

Figure 6. Erosion results for carbon with physical and chemical sputtering.

two. In all, the erosion behavior and the conclusions to be drawn about divertor lifetimes are similar for these cases.

Cases 11-13 show the effect of different plate tilt angles. For these cases the power to the plate is kept constant - the heat flux scales per the Table 1 model. The trend is that a shallower divertor angle has somewhat less central redeposition, but this is more than offset by a lower particle flux. This results in somewhat lower erosion and growth rates. A less-tilted plate has a converse effect. The choice of a plate tilt angle would probably be dictated more by the peak heat flux and by geometric considerations e.g. He pumping behavior, than by erosion considerations.

The erosion variations due to tilt angle has implications for the time-dependent variation in erosion behavior. This was assessed briefly as follows: Fig. 7 shows the original divertor plate shape (i.e. a straight line) and the shape resulting from the net erosion profile of Fig. 4 applied to a burn time of t = .04 burn·yr. At this time a maximum erosion of about 1 cm has occurred. The field line-to-plate angles, that were 20° originally, change as shown. This changes the particle flux. Although REDEP runs were not made for the new shape we conclude from cases 11-13 that the erosion rates should be reasonably similar (assuming unchanged plate region plasma conditions). Therefore, the REDEP results for t = 0 should provide a reasonable guidance for lifetime calculations.

5.4 Plasma Contamination

The REDEP calculations provide an estimate of core plasma contamination by sputtering. This is done by computing the ratio of the sputtered atom current leaving the divertor plate vicinity (y > 3 cm) to the D-T ion current entering the plate vicinity. This parameter, "f_z" represents an upper bound to the core plasma concentration, n_C/N_{DT}, for equilibrium conditions.

For the reference case, $f_z = 1.4 \times 10^{-3}$; this rises to $f_z = 4.6 \times 10^{-3}$ for case 10. For a computation made with reference case parameters except that y = 1 cm was set as the carbon loss-to-plasma limit, $f_z = 7.1 \times 10^{-3}$. The latter is a conservative case as regards core contamination. It appears then that core plasma contamination from divertor sputtering should be low, in spite of the high erosion rates. This is simply due to the short mean free paths for sputtered atom ionization, compared to the distances necessary for

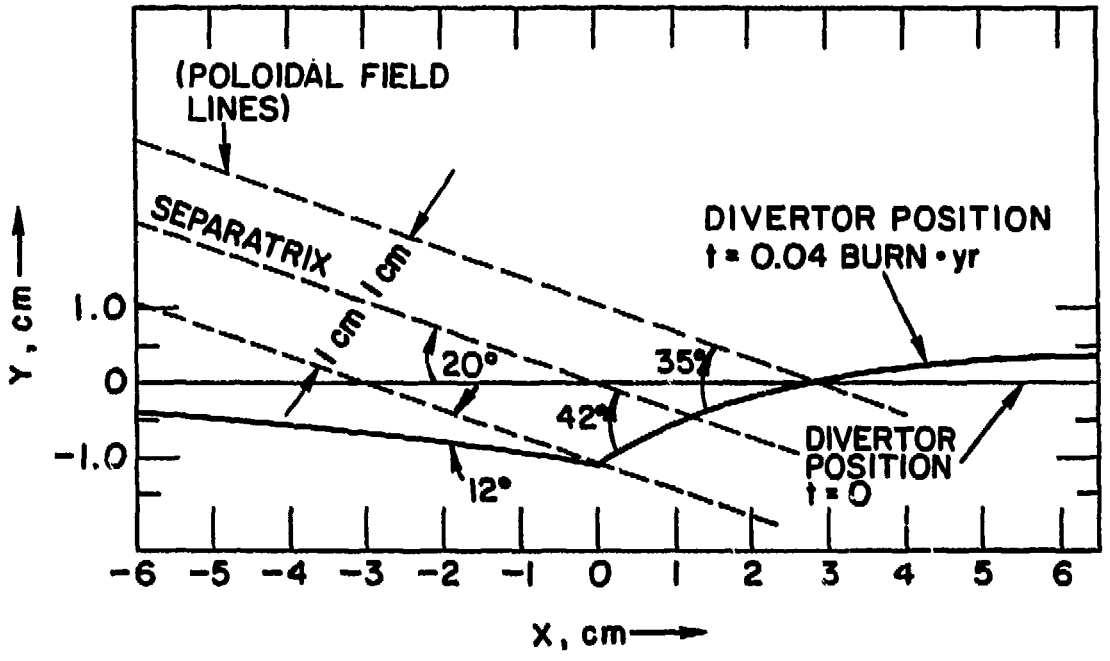

Figure 7. Divertor shape initially and after undergoing erosion. For a carbon plate under reference conditions.

an atom to reach the core plasma.

Another potential source of plasma contamination is by charge exchange sputtering of the first wall. Some first wall sputtered material, traversing through the scrapeoff zone, can enter the core plasma. Subsequent transport to the divertor plate can occur. Impurities from this source would impinge on the divertor plate with higher energies than divertor-region-ionized material (due to generally higher charge states and flow velocities). To assess the effect of wall sputtered material on divertor erosion, computer runs were made using several, fairly high, core concentrations of carbon, assumed to arise from carbon first wall sputtering. The net erosion rate for cases are shown in Fig. 8. The reference case ($f_z \approx 0$) is also shown for comparison. The enhanced carbon in the core appears simply to result in extra deposition on the divertor plate. The net erosion rate is reduced and the growth rate is consequently increased. (Conceivably, divertor plate erosion could be reduced or "repaired" by selective injection of carbon into the core or scrapeoff zone, if such injection could be tailored to result in tolerable growth rates.)

5.5 Beryllium

The advantages of a beryllium coating over carbon include the following: no chemical sputtering or radiation enhanced sublimation, potentially much better mechanical properties of the redeposited surface, and less tritium retention. Potential disadvantages concern the thermal properties and disruption response. REDEP results for a beryllium coated divertor plate are shown in Fig. 9 and Table 2. It should be noted that the analysis uses a cruder sputtering model for beryllium than for carbon. In particular, more information is needed about sheath effects on Be ion angles of incidence, sputtered distributions for oblique incidence, and the effect of a hydrogen surface concentration, if any.

The erosion results for beryllium are qualitatively similar to carbon. Both gross and net erosion rates are high, with the net rate being an order of magnitude lower than the gross rate. The plasma contamination parameter is similar.

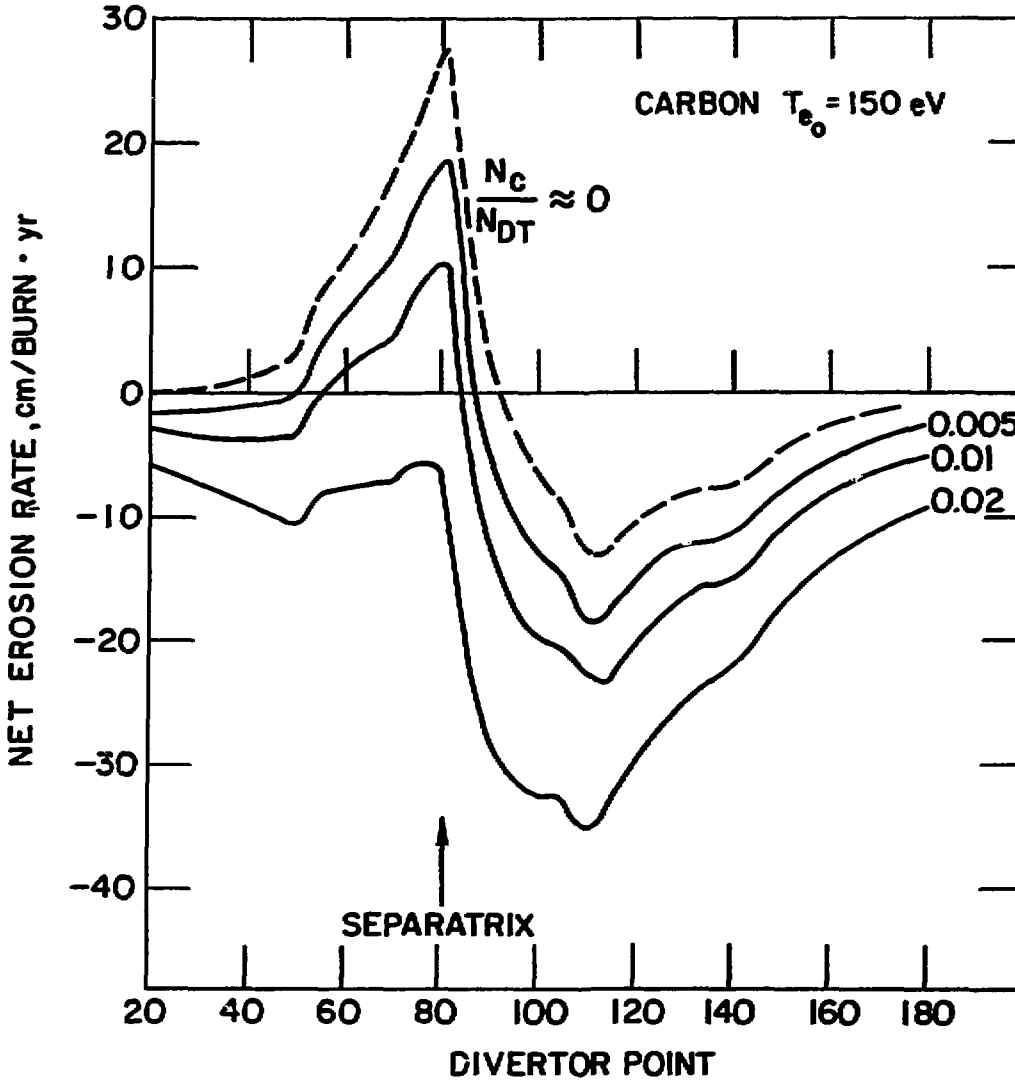

Figure 8. Effect of a high carbon concentration in the plasma core resulting from wall erosion (or other source) on the divertor plate erosion.

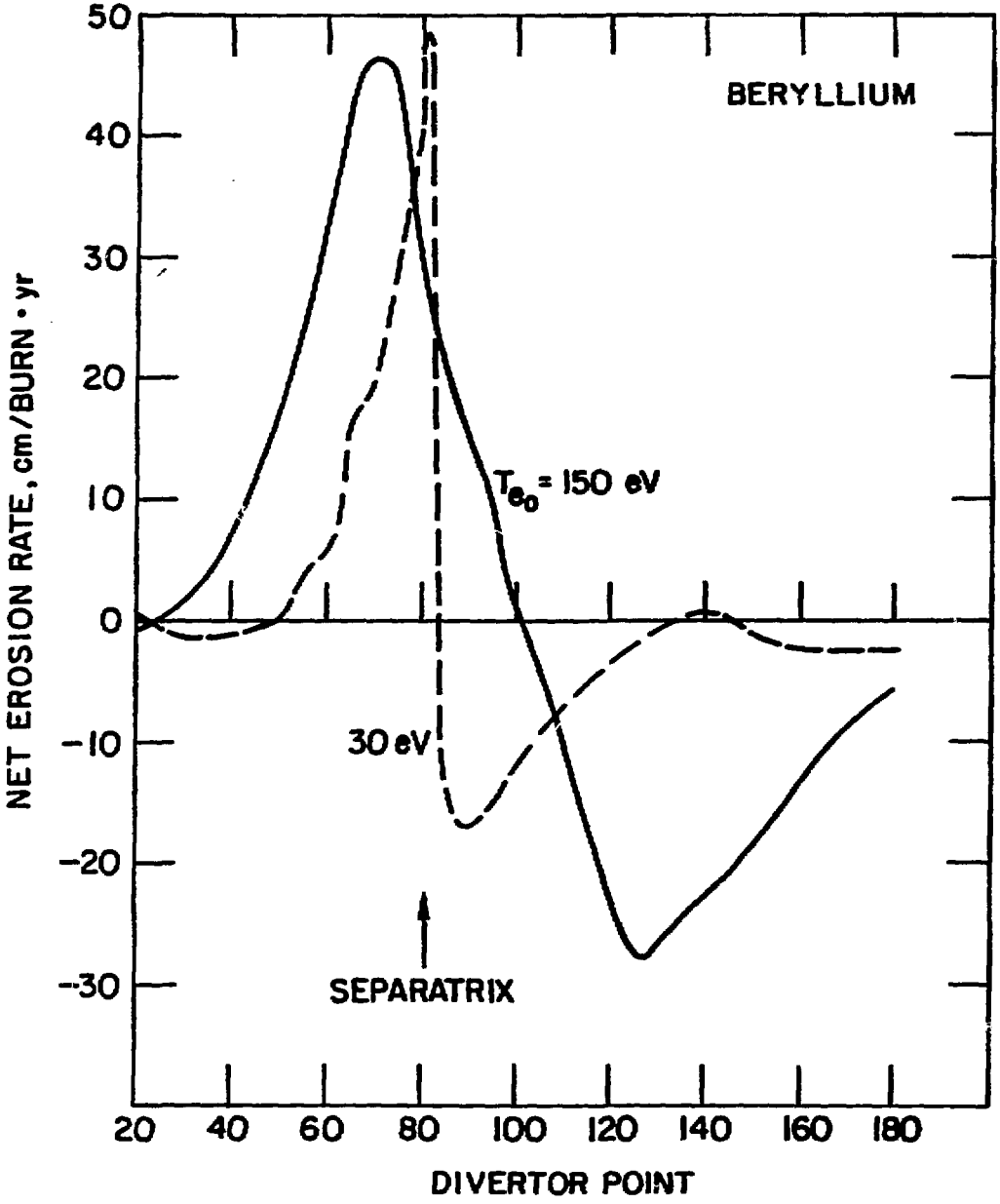

Figure 9. Erosion of a beryllium coated divertor plate.

The tritium surface concentration in beryllium is uncertain but it generally appears experimentally to be much less than for carbon.[17] To provide a rough idea of the difference between beryllium and carbon, tritium co-deposition rates for beryllium were computed using a ratio of T/Be = .02. As shown in Table 2, the resulting tritium retention rates are considerably less than for carbon but are still significant.

5.6 Tungsten

The key issue for a tungsten (or other high Z) divertor plate is the edge plasma temperature limit due to self-sputtering limitations.[4] This limit depends on the sheath potential, charge state of the redeposited ions, and the energy at which the self-sputtering coefficient reaches unity. Based on existing parameter estimates for tungsten,[2] the plasma temperature limit, at the divertor sheath, is about 50 eV. This is subject to considerable uncertainty and may prove to be conservative. In any event, for plasma temperatures below the self-sputtering limit, a tungsten plate appears to work well. This is illustrated in Fig. 10 for a W plate at T_{e_o} = 40 eV.

For this case there is no D-T sputtering. All sputtering is due to helium (doubly charged) plus self-sputtering. Erosion rates are very low, as is tritium co-deposition (computed using a ratio of T/W = .02) The plasma contamination fraction is essentially zero.

5.7 Effect of Sweeping

To reduce the peak heat and particle flux to the divertor plate it has been proposed to sweep the poloidal field lines near the divertor. Sweeping would be accomplished via current oscillation in appropriate divertor coils. For erosion the sweep frequency is immaterial since redeposition occurs at ~1 μs time scales - much shorter than any possible sweep period. Moving the separatrix strike point at fixed intervals, e.g. every 100 shots, would be equally effective in reducing erosion, as in-pulse sweeping.

The effect of sweeping on erosion has been analyzed by computing the time-averaged net erosion rate for a linear (saw-tooth) sweep. This is given as follows:

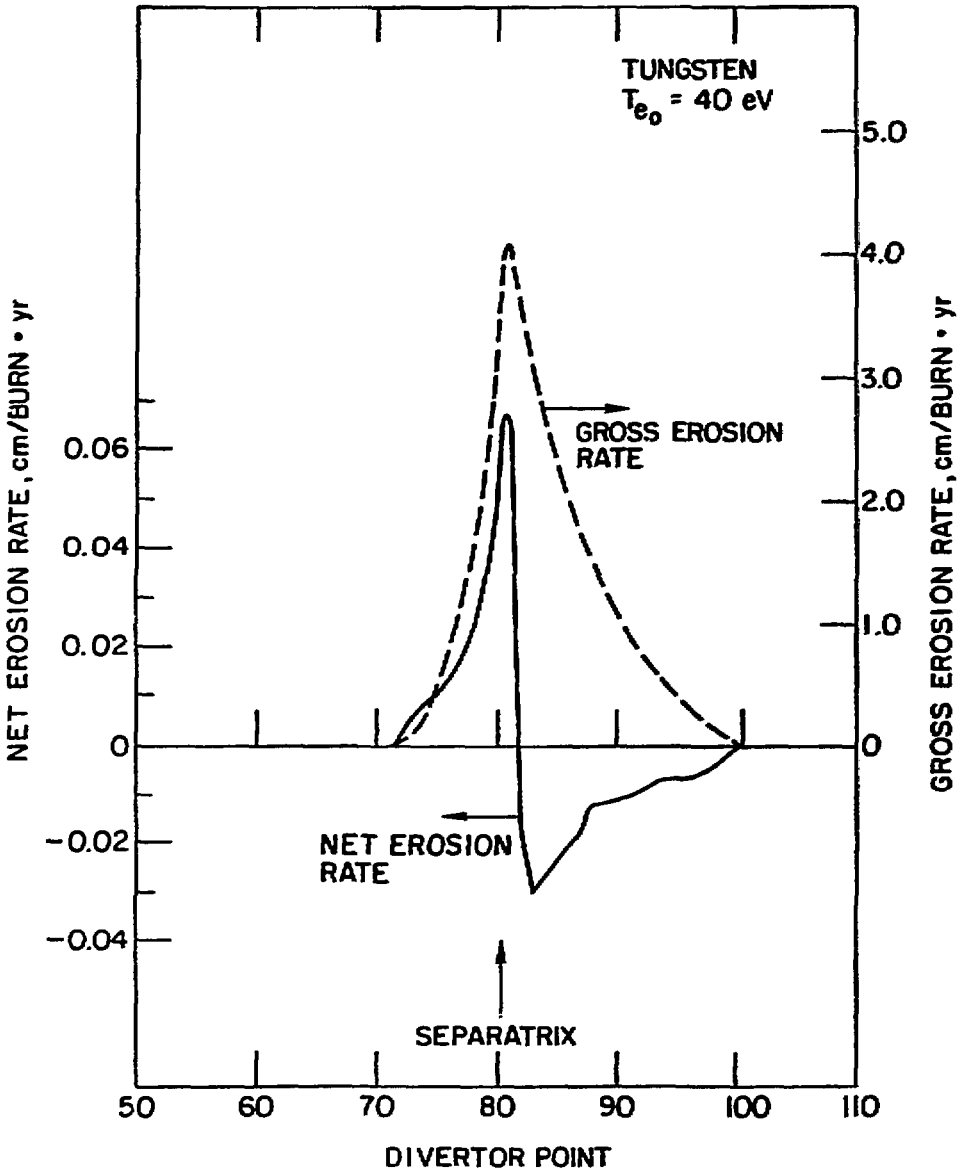

Figure 10. Erosion of a tungsten coated divertor plate.

$$\bar{\Gamma}_z^{NET}(x) = \frac{1}{2L}\int_{-L}^{L} \Gamma_z^{NET}(x + x')\,dx' \qquad (3)$$

where Γ_z^{NET} is the net erosion rate for the no-sweep condition, and the sweep distance along the divertor plate is ± L. Equation (3) was evaluated for the carbon plate reference case, for various sweep distances. The results are shown in Fig. 11 and cases 18-20 of Table 2.

Sweeping results in a significant reduction in erosion. Peak erosion rates are reduced by factors of about 2, 4, 8 for sweep distances of ± 5 cm, ± 10 cm, and ± 20 cm respectively. Tritium co-deposition is also reduced although by not as much. A similar reduction in erosion would clearly be obtained for beryllium.

5.8 Lifetime

The erosion lifetime of the divertor plate is determined by the net sputtering rate and by disruption erosion. As an example of the implications of sputtering erosion, Table 3 shows the lifetime of a 1 cm thick divertor plate coating for a variety of conditions. This table is based on the computed peak net erosion rates and the assumption that disruptions erode one half of the coating, leaving .5 cm for the sputtering erosion limit. A duty factor of unity is included to show the implications of sputtering erosion for a commercial fusion reactor. In this case only tungsten would be feasible. For low duty factor operation, ~ 2-10%, multi-month to multi-year operation is apparently possible with the low-Z materials.

6. DISCUSSION

Additional erosion of the divertor may arise from oxygen and/or other plasma contaminants, and in the case of carbon, radiation enhanced sublimation. Oxygen physical sputtering has not been analyzed but should increase the net erosion rate by approximately the ratio of the oxygen sputtering rate to the D+T+He sputtering rate. Chemical sputtering by oxygen, on carbon and high temperature tungsten, is potentially serious, if oxygen recycles rapidly in the near-plate region. Radiation enhanced sublimation of carbon will contribute to erosion for surface temperatures $\gtrsim$ 800 C. Although not included in the present calculations, it was recently found[18] that the combination of

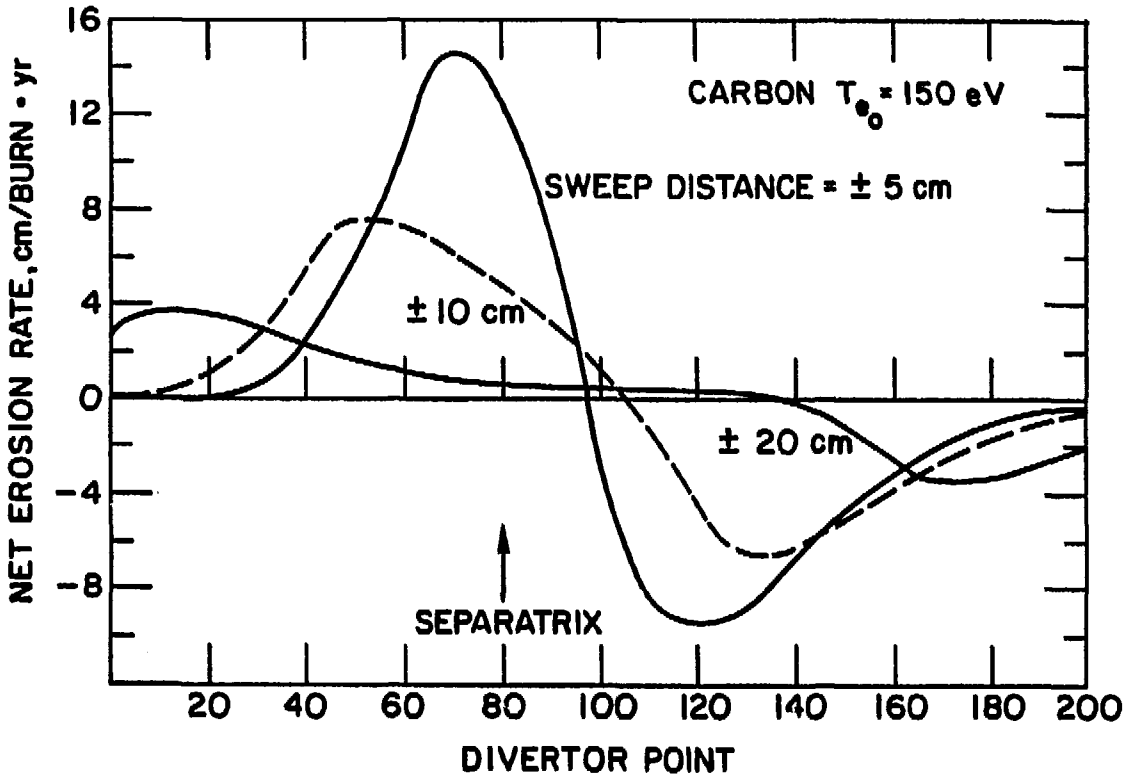

Figure 11. Effect of poloidal field line sweeping on divertor plate erosion; time average net erosion rate as a function of sweep distance.

Table 3. Divertor Plate Lifetime as Set by Sputtering Erosion

Material	Conditions	Duty Factor*	Lifetime**
Carbon	T_{e_o} = 150 eV, phys. sputt. only.	1.0 .02	7 calendar days .9 year
Carbon	above with ± 10 cm sweep.	1.0 .02	23 days 3.1 years
Carbon	T_{e_o} = 150 eV, chem. sputt., ± 10 cm sweep.	1.0 .02	8 days 1.1 years
Beryllium	T_{e_o} = 150 eV, ± 10 cm sweep.	1.0 .02	13 days 1.8 years
Tungsten	T_{e_o} = 40 eV, (no sweep).	1.0 .02	7 years 350 years

* Burn time/calendar time.

** Time to erode 0.5 cm of material based on peak net erosion rates -- all times in calendar units.

radiation enhanced sublimation and physical self-sputtering can significantly limit the permissible operating temperature of a carbon divertor surface.

7. CONCLUSIONS

Sputtering erosion of the ITER divertor has been examined for the reference carbon coating as well as for beryllium and tungsten alternatives, and for a variety of plasma edge conditions. The analysis has used the REDEP computer code with recently developed information and models on oblique angle sheath conditions, sputtering coefficients of hydrogen containing carbon, and sputtered particle distributions. A parametric model of the near-plate plasma, based on plasma transport code simulations, has also been developed and employed in the analysis. Although the ITER design will of course evolve, the present results should provide reasonable guidance for material selection, edge temperature optimization, and divertor plate engineering. The results should be relevant to fusion reactors post ITER as well.

A carbon coated divertor plate suffers from high net erosion rates and potentially high co-deposited tritium retention rates. Chemical sputtering increases net erosion considerably (~ a factor of 3) over physical sputtering. The use of a carbon surface appears to be very questionable for "technology phase" ITER operation (moderate to high duty factor) let alone for a commercial reactor. Nevertheless, carbon may permit acceptable operation for low duty factor (2-10%) "physics phase" operation. This latter conclusion is subject to the requirement that the redeposited carbon has acceptable mechanical and sputtering properties - an issue requiring experimental assessment. Carbon performs better at low edge temperatures (~ 30 eV) than at medium temperatures (~ 150 eV) from the standpoint of sputtering, but probably not better enough to make a qualitative difference in its usefulness. Similarly, the erosion results are relatively insensitive to changes in temperature and density profiles, and poloidal field angles.

Divertor poloidal field sweeping results in a substantial reduction in erosion. Sweeping, for erosion control purposes, is easier than for power control, since the sweep frequency is not important, e.g., the strike point could be changed once a day. Sweeping, therefore, is attractive for reducing low-Z coating erosion. Sweeping, however, may involve tradeoffs with other divertor requirements such as helium pumping.

Beryllium has higher net erosion rates than physically-sputtered-only carbon, but similar rates to physically and chemically sputtered carbon. Beryllium, being a metal, has less questionable redeposited material properties than carbon, and in-situ recoating of eroded areas may be possible. Tritium retention in beryllium is predicted to be substantially less than for carbon. More data, however, is needed on tritium retention properties of beryllium and, in particular, on self-sputtering for glancing magnetic angle sheath conditions, for a more confident assessment of the potential for a beryllium divertor surface.

In spite of the high erosion rates of carbon and beryllium, the REDEP code predicts that very little C or Be reaches the plasma core. Essentially, erosion results from a redistribution of plate material, generally from the inboard to the outboard major radius side of the (outer) divertor plate. Few sputtered atoms reach even a centimeter or so from the plate, for the high recycling divertor regime. The core concentration, of sputtered C or Be, is predicted to be on the order of several tenths of a percent.

As found in previous studies, tungsten is clearly preferred for erosion at low plasma edge temperatures. At a 40 eV plasma plate temperature a tungsten coated plate would permit multi-year continuous operation with essentially zero predicted plasma contamination. Tungsten, however, will be unacceptable at plasma temperatures where the redeposited W ions are energetic enough to cause runaway self sputtering ($Y_{W \leftarrow W} \geq 1$). More work is needed on modeling the transport of sputtered tungsten atoms in the vicinity of a high recycling, oblique field boundary region, in order to develop estimates for the maximum edge temperature possible with a W divertor surface.

Much additional modeling work needs to be done for erosion predictions. Near-term work includes continued comparsion of the REDEP code with experiments, modeling of oxygen and other contaminant effects, and the above-mentioned work on ion boundary transport. In the experimental area there is an ongoing critical need for boundary transport phenomena measurements such as sputtered ion charge states, and for properties of redeposited material, particularly for oblique incidence sputtering coefficients.

8. ACKNOWLEDGEMENT

I would like to thank Dr. A. Hassanein for generating ITMC code data and for his assistance with the carbon chemical sputtering model.

REFERENCES

1. "International Thermonuclear Experimental Reactor (ITER)," IAEA, Vienna (1988).

2. J.N. Brooks, Nuc. Tech./Fusion 4 (1983) 33.

3. R.T. McGrath et al., J. Nuc. Mat., 145-147 (1987) 660.

4. J.N. Brooks et al., J. Nuc. Mat., 163-165 (1989).

5. R.T. McGrath and J.N. Brooks, J. Nuc. Mat. 163-165 (1989).

6. B. Braams, Princeton Plasma Physics Laboratory, Personal Communication (1989).

7. M. Harrison, Culham Laboratory, Personal Communication (1989).

8. S. Cohen, Princeton Plasma Physics Laboratory, Personal Communication (1989).

9. R. Chodura, Phys. Fluids 25 (1982) 1628.

10. A.B. DeWald, A.W. Bailey, and J.N. Brooks, Phys. Fluids 30 (1987) 267.

11. K.L. Wilson and W.L. Hsu, J. Nuc. Mat. 145-147 (1987) 121.

12. D.L. Smith et al., Proc. 9th Symposium on Engineering Problems of Fusion Research, IEEE PUB #81CH1715-2 (1981) 719.

13. A. Hassanein, Nuc. Inst. and Meth. Phys. Res., B13 (1986) 225.

14. M. Thompson, Philos. Mag., 18, 377 (1968).

15. A.E. Pontau, R.A. Causey and F. Bohdansky, J. Nuc. Mat. 145-147 (1987) 775.

16. J. Roth, J. Nuc. Mat. 145-147 (1987) 87.

17. K. Wilson, Sandia National Laboratory, Personal Communication (1989).

18. J.N. Brooks, "Temperature Limit of a Graphite Divertor Surface Due to Particle Erosion," Argonne National Laboratory Report, ANL/FPP/TM-236 (1989).

DISTRIBUTION LIST FOR ANL/FPP/TM-242

Internal

M. Billone
J. Brooks (10)
O. Chopra
R. Clemmer
D. Ehst
K. Evans
P. Finn
Y. Gohar
L. Greenwood
D. Gruen
A. Hassanein
T. Hua
A. Hull
C. Johnson
A. Krauss
B. Loomis
S. Majumdar
R. Mattas
B. Picologlou
K. Porges
C. Reed
D. Smith
D. Sze
L. Turner
FPP Files (25)
ANL Contract File
ANL Library
ANL Patent Dept
TIS Files (3)

External

DOE-OSTI, for distribution per UC-420 (37)
Manager, Chicago Operations Office
C. Baker, Oak Ridge National Laboratory
R. Causey, Sandia National Laboratory, Livermore
M. Cohen, Office of Fusion Energy, DOE
S. Cohen, Princeton Plasma Physics Laboratory
A. Dewald, Georgia Institute of Technology
K. Dimoff, Institute National de La Recherche Scientifique
B. Doyle, Sandia National Laboratory, Albuquerque
H.F. Dylla, Princeton Plasma Physics Laboratory
A. Haasz, University of Toronto
M. Harrison, Culham Laboratory
Y. Hirooka, University of California, Los Angeles
W. Hsu, Sandia National Laboratory, Livermore
R. McGrath, Sandia National Laboratory, Albuquerque
R. Nygren, Sandia National Laboratory, Albuquerque
K. Parbhakar, Institut National de la Recherche Scientifique
P. Stangeby, University of Toronto
T. Tomabechi, Japan Atomic Energy Research Institute, Japan
M. Ulrickson, Princeton Plasma Physics Laboratory
K. Wilson, Sandia National Laboratory, Livermore
Bibliothek, Max-Planck-Institute fur Plasmaphysik, West Germany
Bibliothek, Institute fur Plasmaphysik, KFA Julich, West Germany
C.E.A. Library, Fontenay-aux-Roses, France
Librarian, Culham Laboratory, England
Library, Commission of the European Community, Italy
Thermonuclear Library, Japan Atomic Energy Research Institute, Japan